Desalination and Water Treatment
www.deswater.com

doi: 10.5004/dwt.2021.27395

229 (2021) 430–440
July

Eucalyptus sawdust as an alternative adsorbent for rhodamine B dye removal

Leticia dos Reis Darcie, Brenna Vieira Jacon, Grazielle Santos Silva Andrade*, Anderson Maida Siqueira Oliveira, Melina Savioli Lopes, Tania Regina Giraldi

Federal University of Alfenas (UNIFAL), Rodovia José Aurélio Vilela, 11999, Poços de Caldas, MG 37715-400, Brazil, Tel. +55 35 3697-4600; emails: grazielle.andrade@unifal-mg.edu.br (G.S. Silva Andrade), leticia_darcie@hotmail.com (L. dos Reis Darcie), brenna.v.jacon@gmail.com (B.V. Jacon), andersonmaida@usp.br (A.M. Siqueira Oliveira), melina.savioli@unifal-mg.edu.br (M.S. Lopes), tania.giraldi@unifal-mg.edu.br (T.R. Giraldi)

Received 27 November 2020; Accepted 5 May 2021

ABSTRACT

This paper describes the decoloration potential of a low-cost natural adsorbent, eucalyptus sawdust (ES), for rhodamine B (RhB) removal. Fourier-transform infrared spectroscopy analysis of the adsorbent revealed the presence of characteristic groups of cellulose, hemicellulose, and lignin. Scanning electron microscopy images showed that the surface of ES is heterogeneous and irregular. Point of zero charge studies revealed a negatively charged surface, which is favorable for RhB adsorption. A 2^3 full factorial central composite rotatable design was used to optimize dye removal. The optimal conditions were found to be biomass dosage of 0.49%, particle size of 0.44 mm, and unadjusted pH (4.0), providing high adsorption capacity and removal percentage. Adsorption studies were conducted using RhB concentrations of 50 and 100 mg L^{-1}; under these conditions, the maximum adsorption was 90.1% and 92.8%, respectively, and the equilibrium was established in 420 min. Isothermal data were fitted to the Langmuir model, revealing a maximum adsorption capacity of 29.94 mg g^{-1}. The rate of adsorption followed second-order kinetics, indicating the occurrence of a chemical phenomenon and diffusion as the rate-governing step. Thermodynamic parameters showed that RhB adsorption is endothermic, spontaneous, and favorable.

Keywords: Adsorption; Lignocellulosic biomass; Statistical analysis; Dyes; Eucalyptus sawdust

1. Introduction

Adequate management and use of water resources are one of the most important aspects for the sustainable development of modern societies. Most industrial processes that use water generate toxic effluents and/or effluents with high microbial activity, which are therefore unsuitable for reuse in agriculture or human activities. Rhodamine B (RhB) is an important contaminant with carcinogenic, genotoxic, and neurotoxic properties. Ingestion of the dye is harmful to humans because its carboxyl group interacts with the DNA backbone, forming intermolecular hydrogen bonds that affect DNA function [1]. Despite its toxicity, RhB is still used in textile industries for its intense and stable color and added to herbicides as a tracking agent.

Water treatment has attracted considerable attention during the last decades [2–6]. Textile manufacturing is an example of industrial activity that generates large quantities of contaminated effluents. Textile wastewater typically contains organic contaminants, as most industrial dyes contain organic functions. Several physical and chemical processes have been used to treat textile wastewaters. The most used physical processes include adsorption and coagulation–flocculation [7–9].

Adsorption is widely applied to remove pollutants from dye wastewater because of its many advantages,

* Corresponding author.

including easy operation, low cost, and high efficiency [10]. Several studies on the adsorption of pollutants from wastewater containing dyes have been carried out with a wide range of materials as adsorbents, such as activated carbon [11], ZnO [12], zeolites [13], carbon xerogels [14], microalgae [15], silica [16,17], seed hulls [18], and lignocellulosic biomass [19].

Many researchers have used synthetic materials for RhB adsorption. Abdulrazak and Rohani [13] investigated RhB removal by using Fe_2O_3 supported zeolite nanoparticles. Particles were synthesized and modified by sodium dodecyl sulfate. The Freundlich isotherm model showed a good fit to experimental data, revealing a maximum adsorption capacity of 89.3 mg g^{-1}. Tuzen et al. [11] obtained activated carbon from waste tires and modified it with bimetallic (Fe and Ce) nanoparticles. This nanocomposite was used for RhB removal from aqueous solutions. Adsorption data were well explained by the Langmuir isotherm model, and the maximum adsorption capacity was 324.6 mg g^{-1}. Ptaszkowska-Koniarz et al. [14] synthesized carbon xerogels by resorcinol and formaldehyde polycondensation. Xerogels were subjected to surface oxidation with ammonium persulfate, amine functionalization, and/or impregnation with copper(II) chloride. All carbon xerogels were used for RhB adsorption from aqueous solutions. The maximum adsorption capacities of the samples ranged from 91 to 132 mg g^{-1}. The most effective adsorbent for RhB proved to be the sample modified with amine groups and copper(II) chloride.

Lignocellulosic biomass has a high capacity to attract and bind pollutant ions because of its various functional groups, such as hydroxyls and carboxylic acids [19,20]. This characteristic has stimulated the use of lignocellulosic materials as biosorbents for the removal of environmental pollutants, including dyes [21] and heavy metal ions [22]. As an example, Jain and Gogate [23] used *Prunus dulcis* leaves to adsorb the dyes Acid Green 25 and Acid Blue 113 [24,25]. Modern agricultural industries produce millions of tonnes of waste and byproducts that show potential as useful resources. Agroindustrial residues (organic materials produced as byproducts of the harvesting and industrial processing of agricultural crops) are a promising alternative to traditional adsorbents, as they are low-cost, readily available, highly sorptive, easily modifiable, insensitive to toxic substances, and easy to manipulate during treatment [26]. Eucalyptus sawdust (ES) is a common agroindustrial waste of the pulp and paper industry and an abundant natural resource [27] rich in cellulose [28]. The high daily production of ES may pose an environmental risk [27,29]. ES constituents, namely lignin, cellulose, and hemicelluloses, contain a variety of functional groups (e.g., hydroxyls and carboxylic acids) that can act as adsorptive sites, suggesting the potential of ES as bioadsorbent [19,20].

This study aimed to describe the mechanism of RhB dye removal from aqueous solutions using ES as adsorbent. The effects of solution pH, biosorbent dosage, initial dye concentration, temperature, and contact time were evaluated. Additionally, kinetic, equilibrium, and thermodynamic parameters were investigated for a greater understanding of the adsorption process.

2. Methods

2.1. Materials

Sawdust from *Eucalyptus globulus* was obtained in Tapiratiba, São Paulo State, Brazil. Before use, the material was dried under sunlight for 48 h and then oven-dried at 60°C for about 24 h, until constant weight was achieved. ES was ground and sieved through Tyler sieves to obtain fractions with average particle sizes of 0.44, 0.35, 0.25, 0.15, and 0.06 mm. The relative proportion of each fraction was determined by measuring the weight of material retained in each sieve.

2.2. ES characterization

Biosorption mechanisms can be varied but are predictable from sorbent surface characteristics and associated functional groups. ES was evaluated for specific surface area by N_2 physisorption, for stability in aqueous suspension by point of zero charge studies, for organic functions by Fourier-transform infrared spectroscopy (FTIR), and for surface morphology by scanning electron microscopy (SEM).

N_2 physisorption was performed using a Micromeritics Gemini® VII equipment. About 500 mg of sample was completely dried under vacuum at 100°C in a Micrometrics VacPrep 061 Sample Degas System. Measurements were taken, and the specific surface area and average pore size of each sample were calculated from N_2 physisorption isotherms by the Brunauer–Emmett–Teller method.

The point of zero charge (pH_{pzc}) was determined by the powder addition method. First, 20 mL of an electrolyte solution (0.1 M NaCl) was prepared. The solution pH was varied from 2 to 10 using HCl and NaOH solutions (both at 0.1 M). Then, 0.2 g of ES was added to the solutions, which were placed in an orbital shaker incubator at 250 rpm and 30°C for 24 h. After this, the solutions were filtered and the final pH of each sample was recorded.

FTIR measurements were performed by placing ES samples directly on an Agilent Cary 630 spectrometer equipped with an attenuated total reflectance probe. Spectra were recorded over the wavenumber range of 4,000 to 500 cm^{-1} at a resolution of 4 cm^{-1}.

SEM images were acquired on a JEOL JSM 6701F SEM in secondary electron mode at 500× and 2,000× magnification and a working distance of 13 mm. A tungsten cathode was used as electron source at an acceleration voltage of 5 to 10 kV.

2.3. Central composite rotatable design

A central composite rotatable design was performed using a 2^3 full factorial, with 6 axial points and 4 repetitions of the center point, totaling 18 runs. The independent variables were particle size, pH, and biomass dosage. The response variables were adsorption capacity (q_t) and dye removal percentage (R%). Table 1 shows the actual and coded values used in the experimental design.

All tests were carried out using 50 mL of an RhB solution at 100 mg L^{-1}. Solution pH, particle size, and biomass dosage were varied according to the experimental design matrix. When necessary, the pH was adjusted using 0.1 M

Table 1
Independent variables, codes, and levels used in the experimental design

Independent variable	Code	−1.68	−1	0	+1	+1.68
Particle size (mm)	X_1	0.06	0.15	0.25	0.35	0.44
Solution pH	X_2	2.00	3.62	6.00	8.38	10.00
Biomass dosage (%)	X_3	0.10	0.49	1.05	1.61	2.00

NaOH or 0.1 M H_2SO_4. Flasks were incubated for 24 h in an orbital shaker incubator at 30°C and 150 rpm. After the adsorption equilibrium was reached, solutions were centrifuged and the residual RhB concentration measured using a UV-Vis spectrophotometer at 554 nm. Biosorbent adsorption capacity (q_t, mg g^{-1}) and dye removal percentage (R%) were calculated by Eqs. (1) and (2), respectively.

$$q_t = \frac{\left(C_0 - C_f\right)V}{m} \tag{1}$$

$$R\% = \frac{C_0 - C_t}{C_0} \times 100 \tag{2}$$

where C_0 is the initial RhB concentration (mg L^{-1}), C_f is the final RhB concentration (mg L^{-1}), V is the volume of solution (L), and m is the mass of biosorbent (g).

Experimental data were analyzed using Statistica® software to assess the influence of each variable on the adsorption process and determine the optimal conditions for RhB adsorption on ES. A quadratic interaction model was applied to estimate the mean values of the analyzed variables and their interaction effects. Models describing adsorption capacity and removal percentage were obtained from regression coefficients. Then, analysis of variance (ANOVA) was performed to assess the goodness of fit of each model. The level of significance was set at 5% ($p < 0.05$).

2.4. Adsorption kinetics

ES with a particle size of 0.44 mm was added at 0.49% to 50 mL of an RhB solution at an initial concentration of 100 mg L^{-1} and natural pH (without adjustment). The solution was stirred at 150 rpm and 30°C in an orbital shaker incubator for 24 h. Samples were collected at 10 time points (0.5, 1.0, 1.5, 2.0, 2.5, 3.0, 4.0, 5.0, and 24 h). Experimental data were fitted to pseudo-first-order [Eq. (3)], pseudo-second-order [Eq. (4)], and intraparticle diffusion [Eq. (5)] models.

$$\frac{dq_t}{dt} = k_1\left(q_e - q_t\right) \tag{3}$$

$$\frac{dq_t}{dt} = k_2\left(q_e - q_t\right)^2 \tag{4}$$

$$q_t = k_3 t^{0.5} + C \tag{5}$$

where q_e is the adsorption capacity at equilibrium (mg g^{-1}) and k_1, k_2, and k_3 are the rates of adsorption for pseudo-first-order, pseudo-second-order, and intraparticle diffusion models, respectively.

2.5. Adsorption isotherms

Adsorption isotherm studies were carried out using a fixed amount (0.49%) of 0.44 mm ES. ES was mixed with 50 mL of a dye solution at pH 4.00 and nine different initial concentrations (20–500 mg L^{-1}) in glass flasks. Flasks were stirred at 150 rpm for 7 h (equilibrium time) until the equilibrium was reached. Langmuir [Eq. (6)] and Freundlich [Eq. (7)] isotherm models were used to estimate RhB adsorption, as follows:

$$q_e = \frac{q_{\max} K_L C_e}{1 + K_L C_e} \tag{6}$$

$$q_e = K_F C_e^{1/n} \tag{7}$$

where $q_{\max}$ (mg g^{-1}) is the maximum adsorption capacity of the biosorbent at equilibrium, C_e (mg L^{-1}) is the dye concentration at equilibrium, and K_L and K_F are the equilibrium constants of Langmuir and Freundlich models, respectively.

2.6. Thermodynamic parameters

Thermodynamic studies were carried out to determine the equilibrium constant, Gibbs energy variation, and variation in enthalpy and entropy. Briefly, 50 mL of dye solution at initial concentrations of 20, 40, 60, 100, or 300 mg L^{-1} and pH 4.00 was mixed with 0.44 mm ES at 0.49% in glass flasks. Flasks were stirred at 150 rpm for 7 h (equilibrium time) at 30°C, 40°C, or 50°C. Adsorption Gibbs energy variation (ΔG°_{ads}), adsorption enthalpy variation (ΔH°_{ads}), and adsorption entropy variation (ΔS°_{ads}) were determined using Eqs. (8)–(10).

$$\Delta G^\circ_{ads} = -RT\ln\left(K_{ads}\right) \tag{8}$$

$$K_{ads} = \frac{C_0 - C_e}{C_e} \tag{9}$$

$$\Delta G^\circ_{ads} = \Delta H^\circ_{ads} - T\Delta S^\circ_{ads} \tag{10}$$

where K_{ads} is the adsorption equilibrium constant.

3. Results and discussion

3.1. ES characterization

The influence of pH on ES surface properties was evaluated by calculating the material's pH_{pzc}, as shown in Fig. 1.

The pH_{pzc} of ES was found to be pH 4.2. This indicates that at this pH there is no repulsive charge zone, and therefore way, the energy barrier (which keeps biomass in repulsion) is decreased. Consequently, settling of biomass occurs. [30]. The material showed low stability in suspension in the entire pH range evaluated, as evidenced by the low absolute pH_{pzc} values. Because of this low stability, it is essential that adsorption studies be carried out under mechanical agitation, as was done in the present study orbital shaker

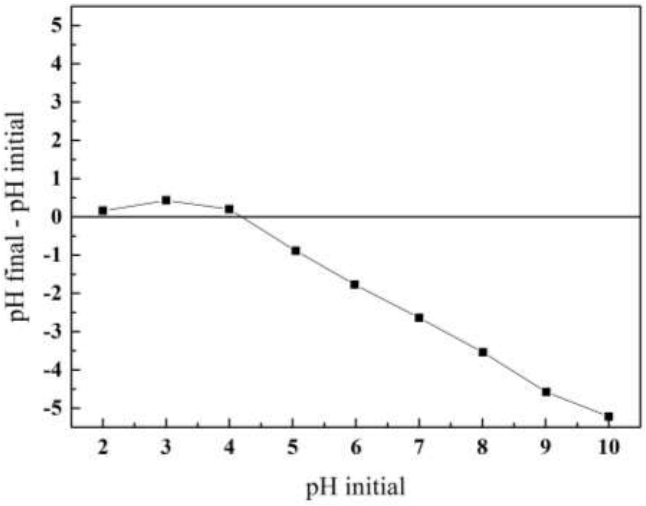

Fig. 1. Point of zero charge of eucalyptus sawdust.

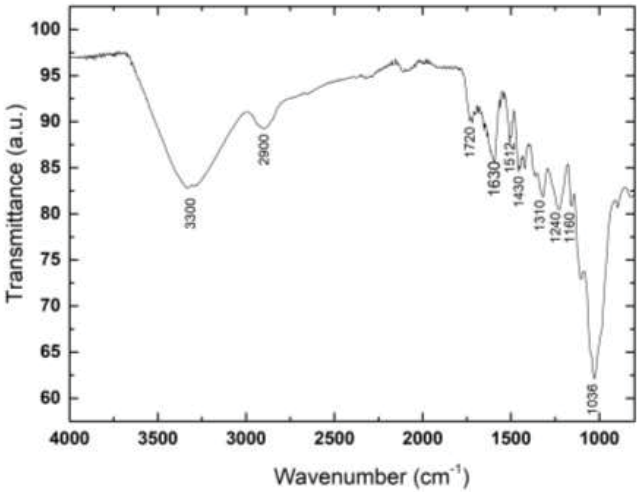

Fig. 2. Fourier-transform infrared spectrum of eucalyptus sawdust.

incubator. In addition, we also observed a predominance of negative surface charges up to pH 10, despite the low stability. Given that RhB is a cationic molecule, its adsorption is favored at pH values above pH_{pzc} (pH 4.2), which promotes electrostatic attraction forces.

Fig. 2 shows the FTIR spectrum of ES.

The main functional groups of ES are described in Table 2.

ES is composed of several useful components, including cellulose, hemicelluloses, lignin, ash, and extractives in a smaller amount. Lignocellulosic materials provide a strong attractive force for the binding of pollutant ions because of their numerous and varied functional groups. As shown in Table 2, ES contained functional groups characteristic of lignin, such as, carboxyl and hydroxyl groups. Such groups are potentially adsorptive, as they have a negative charge, which attracts cationic molecules, such as RhB.

ES morphology was assessed by SEM. SEM images revealed a fibrous material with a highly heterogeneous and irregular surface containing some filaments and grooves (Fig. 3). RhB removal is likely promoted by the presence of external fibers with many filaments and grooves.

N_2 physisorption characterization of ES revealed a specific surface area of 0.7241 $m^2\ g^{-1}$. Although the surface area was low, ES morphology (Fig. 3) indicates that the material can be a good adsorbent; the irregular structure and different porosity levels of ES may facilitate pollutant ion biosorption.

3.2. Central composite rotatable design experiments

Table 3 shows the real and coded values used in the experimental design.

According to Table 3, ES adsorption capacity ranged from 3.96 (run 14) to 47.26 mg g^{-1} (run 13). It is interesting to observe that runs 13 and 14 were carried out using the same biomass particle size and solution pH, indicating that only ES dosage significantly influenced biosorption. The lowest biomass dosage (0.11%) was used in run 13, whereas an 18 times higher dosage (1.99%) was used in run 14. These findings suggest an inverse relationship between biomass dosage and adsorption capacity, as, regardless of solution pH or biomass particle size, an increase in biomass dosage led to a decrease in adsorption capacity. Removal percentage ranged from 57.52 (run 13) to 96.87% (run 15). A removal percentage higher than 87% was obtained in all runs, except run 13. Solution pH and biomass particle size did not seem to influence dye removal percentage. The results of run 13 show that dye removal percentage is markedly reduced by the use of very low biomass dosages. The center point runs afforded similar results, indicating good repeatability of the process. Table 4 shows the effects of parameters on response variables.

Statistical analysis indicated that only the linear and quadratic terms of biomass dosage were significant at $p < 0.05$ for both response variables. Biomass particle size and solution pH, as well as interactions between parameters, did not affect adsorption capacity or dye removal percentage. The negative effect of biomass dosage on adsorption capacity indicates that low values of ES dosage increase adsorption capacity. On the other hand, dye percentage removal increases with ES dosage, as evidenced by the positive effect of the parameter. Such an antagonistic effect between responses was also reported by Souza et al. [31], who used inactivated fungal biomass for dye removal. The authors hypothesized that an increase in biomass dosage leads to an increase in active sites, improving removal efficiency. By contrast, biosorption capacity is related to the concentration gradient between adsorbent and adsorbate, which decreases with increasing biomass levels in the medium.

Eqs. (11) and (12) describe the relationship between response variables and coded individual variables.

$$q_t(Y_1) = 7.72 - 0.07X_1 - 0.68X_2^2 - 0.11X_2 - 0.83X_2^2 - 8.67X_3 + 5.71X_3^2 - 0.01X_1X_2 + 0.08X_1X_3 + 0.14X_2X_3 \quad (11)$$

$$R\%(Y_2) = 96.53 - 0.39X_1 + 0.31X_2^2 - 0.07X_2 + 0.09X_2^2 + 6.89X_3 - 6.01X_3^2 - 0.05X_1X_2 + 0.40X_1X_3 + 0.19X_2X_3 \quad (12)$$

Table 2
Functional groups in eucalyptus sawdust

Band (cm^{-1})	Vibration type
3300	Stretching of O–H bonds in water, cellulose, hemicellulose, and lignin molecules
2900	Stretching of C–H bonds (aliphatic + aromatic) in lignin
1720	Stretching of C=O bonds from aliphatic carboxylic acid and ketones in hemicellulose
1630	Carbonyl stretch (C=O) of hemicellulose acetyl groups and lignin aldehyde groups
1512	Stretching of C=C bonds of the aromatic ring in lignin
1430	CH_2 deformation of cellulose, hemicellulose, and lignin
1310	Vibration of C–H bonds in cellulose and C–O bonds in syringyl
1240	Bending of O–H bonds
1160	Asymmetric stretching of C–O–C bonds in cellulose, hemicellulose, and lignin
1036	Stretching of the C–O bond of ethers and alcohols, confirming the presence of lignin

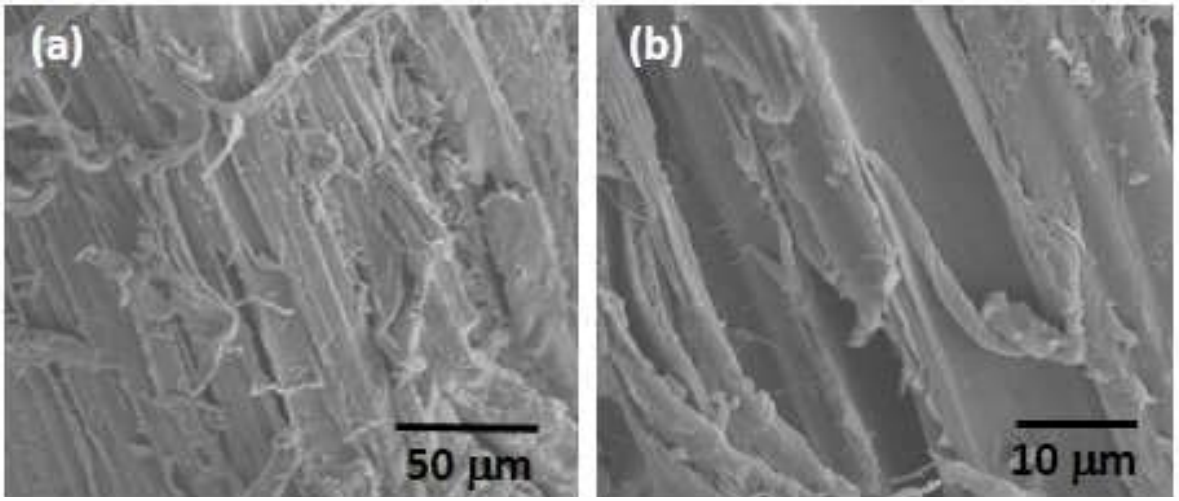

Fig. 3. Scanning electron microscopy images of eucalyptus sawdust at (a) 500× and (b) 2,000× magnification.

where Y_1 is the adsorption capacity (mg g^{-1}), Y_2 is the dye removal percentage (%), X_1 is the coded level of ES particle size (mm), X_2 is the coded level of solution pH, and X_3 is the coded level of ES dosage (%).

The ANOVA table presents the sum of squares, degrees of freedom, *F*-value, and *p*-value for the two models (Table 5). The *F*-test indicated that the two models are predictive and statistically significant at $p < 0.05$. As shown by the correlation coefficients (R^2), the models had a good fit to experimental data, explaining 83.35 and 80.65% of the variability in adsorption capacity and removal percentage, respectively. Thus, regression models were used to generate contour plots (Fig. 4a–d), which allowed determining the optimal region for studying dye removal.

Contour plots clearly demonstrate the antagonistic effect of biomass dosage on adsorptive capacity and dye removal percentage. Fig. 4a shows that, regardless of ES particle size, adsorption capacity increases when using very low amounts of biomass, whereas removal percentage increases proportionally with the increase in biomass from 0.5% onward. A similar behavior was observed for solution pH (Fig. 4b): the parameter did not influence the response variables.

For optimized adsorption, satisfactory values of adsorption capacity and dye removal percentage must be established. Therefore, it is necessary to determine the parameters that satisfy these two conditions. According to the results of statistical analyses and contour plots, a biomass dosage of 0.49% was the most effective in increasing adsorption capacity and removal percentage, as it promoted equilibrium in dye removal. Particle size and solution pH were not assessed for RhB adsorption optimization because they were not statistically significant. It should be noted that 0.44 mm was the prevalent particle size fraction and it was not necessary to adjust the solution pH, as pH values returned to baseline after 2 h of the start of the reaction. Thus, for further dye removal tests, the following optimal conditions were adopted: biomass dosage of 0.49%, biomass particle size of 0.44 mm, and solution pH of 4.0 (unadjusted). Reaction temperature and dye concentration were also evaluated.

3.3. Kinetic studies

Fig. 5 depicts the kinetics of RhB adsorption, showing the effects of contact time between RhB solution and ES adsorbent. RhB adsorption increased until reaching its

Table 3
Experimental design matrix and results for rhodamine B adsorption on eucalyptus sawdust

	Variable (coded value)			Response (coded value)	
Run	Particle size (mm) (X_1)	pH (X_2)	Dosage (%) (X_3)	q_t (mg g^{-1}) (Y_1)	R% (Y_2)
1	0.15 (−1)	3.62 (−1)	0.49 (−1)	16.92	90.42
2	0.35 (+1)	3.62 (−1)	0.49 (−1)	16.62	88.72
3	0.15 (−1)	8.38 (+1)	0.49 (−1)	16.21	89.91
4	0.35 (+1)	8.38 (+1)	0.49 (−1)	15.80	87.51
5	0.15 (−1)	3.62 (−1)	1.61 (+1)	5.09	96.71
6	0.35 (+1)	3.62 (−1)	1.61 (+1)	5.06	96.11
7	0.15 (−1)	8.38 (+1)	1.61 (+1)	4.89	96.46
8	0.35 (+1)	8.38 (+1)	1.61 (+1)	4.87	96.16
9	0.06 (−1.68)	6.00 (0)	1.05 (0)	7.59	94.89
10	0.44 (+1.68)	6.00 (0)	1.05 (0)	7.49	94.68
11	0.25 (0)	2.00 (−1.68)	1.05 (0)	7.00	93.89
12	0.25 (0)	10.00 (+1.68)	1.05 (0)	7.24	94.47
13	0.25 (0)	6.00 (0)	0.10 (−1.68)	47.26	57.52
14	0.25 (0)	6.00 (0)	2.00 (+1.68)	3.96	96.31
15	0.25 (0)	6.00 (0)	1.05 (0)	7.58	96.87
16	0.25 (0)	6.00 (0)	1.05 (0)	7.58	96.87
17	0.25 (0)	6.00 (0)	1.05 (0)	7.57	96.65
18	0.25 (0)	6.00 (0)	1.05 (0)	7.56	96.61

Table 4
Effects of independent variables on adsorption capacity and removal percentage

	Adsorption capacity (mg g^{-1})			Removal percentage (%)		
Variable	E	SE	p-value	E	SE	p-value
Mean	7.72	2.50	0.0150	96.53	2.94	<0.0001
X_1	−0.14	2.71	0.9613	−0.78	3.19	0.8120
X_{21}	−1.36	2.82	0.6417	0.61	3.31	0.8586
X_2	−0.22	2.71	0.9368	−0.14	3.19	0.9665
X^2_2	−1.66	2.82	0.5722	0.18	3.31	0.9576
X_3	−17.35	2.71	0.0002	13.78	3.19	0.0025
X^2_3	11.41	2.82	0.0037	−12.03	3.31	0.0067
X_1X_2	−0.02	3.55	0.9945	−0.10	4.17	0.9814
X_1X_3	0.17	3.55	0.9640	0.80	4.17	0.8525
X_2X_3	0.29	3.55	0.9379	0.38	4.17	0.9296

E, effect; SE, standard error. Significant variables are shown in bold ($p < 0.05$)

maximum value at 420 min for both analyzed concentrations. The adsorption/desorption equilibrium was reached during this period; after this time, the adsorption percentage remained practically constant and the maximum dye adsorbed was 92.8% for the 100 mg L^{-1} RhB solution and 90.1% for the 50 mg L^{-1} RhB solution (Fig. 5a). Therefore, the previously determined reaction time of 420 min was adequate for investigating the kinetics of RhB adsorption.

Pseudo-first-order, pseudo-second-order, and linearized intraparticle diffusion kinetic models were fitted to experimental data, and the results are presented in Fig. 6 and Table 6. The pseudo-second-order kinetic model better described RhB adsorption, with R^2 values close to 1.0 (0.9998 and 0.9999) for both dye concentrations. The estimated equilibrium adsorption capacity was 17.24 and 8.67 mg g^{-1} for initial dye concentrations of 100 and 50 mg L^{-1}, respectively.

3.4. Adsorption isotherm

Adsorption isotherm studies were carried out to determine the quantity of RhB removed per unit mass of ES.

Table 5
ANOVA for the adsorption of rhodamine B on eucalyptus sawdust

	Adsorption capacity (mg g^{-1})				Removal percentage (%)			
Source of variation	SS	DF	F-value	p-value	SS	DF	F-value	p-value
Regression	1,526.02	9	6.74	0.0066	1,158.00	9	3.71	0.0393
Residual	201.18	8			277.762	8		
Total	1,727.20	17			1,435.760	17		
R^2	83.55%				80.65%			

SS, sum of squares; DF, degrees of freedom

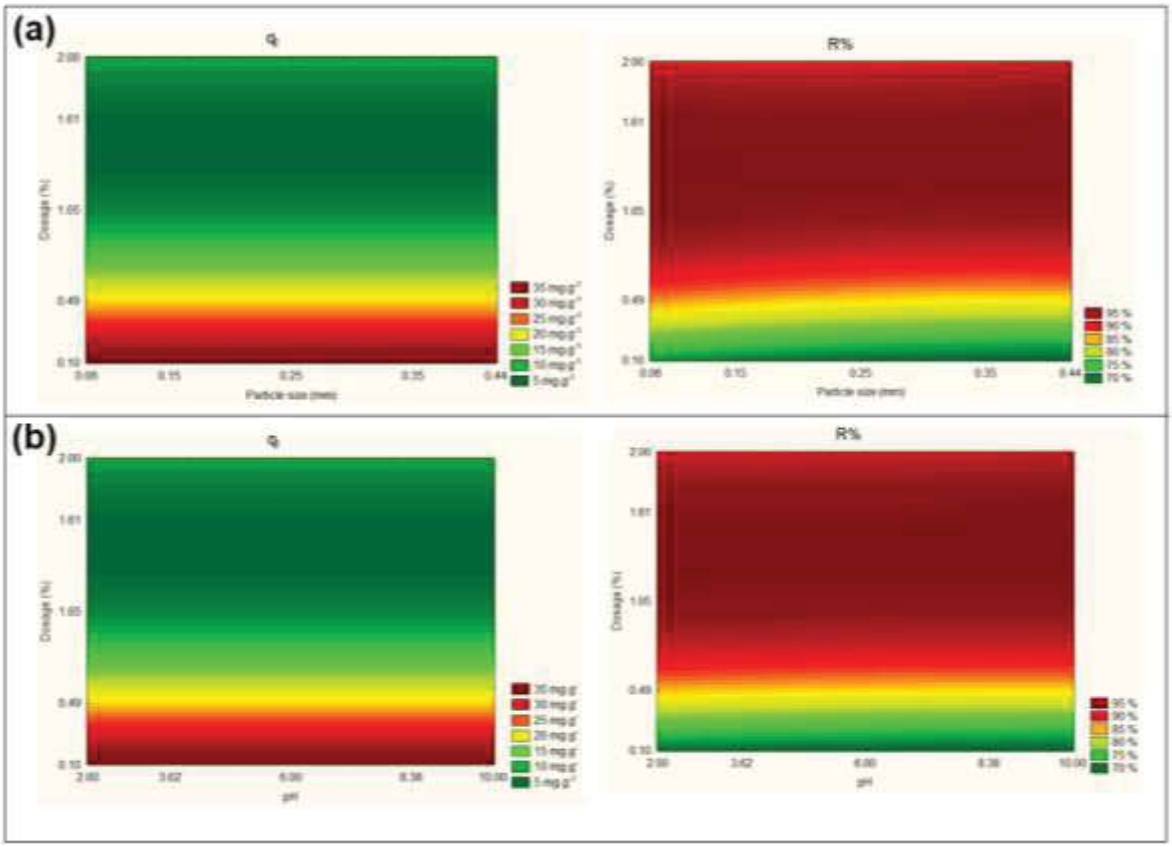

Fig. 4. Contour plots for the rhodamine B adsorption process. Effects of (a) particle size plus dosage and (b) pH plus dosage on adsorption capacity (q_t) and removal percentage (R%).

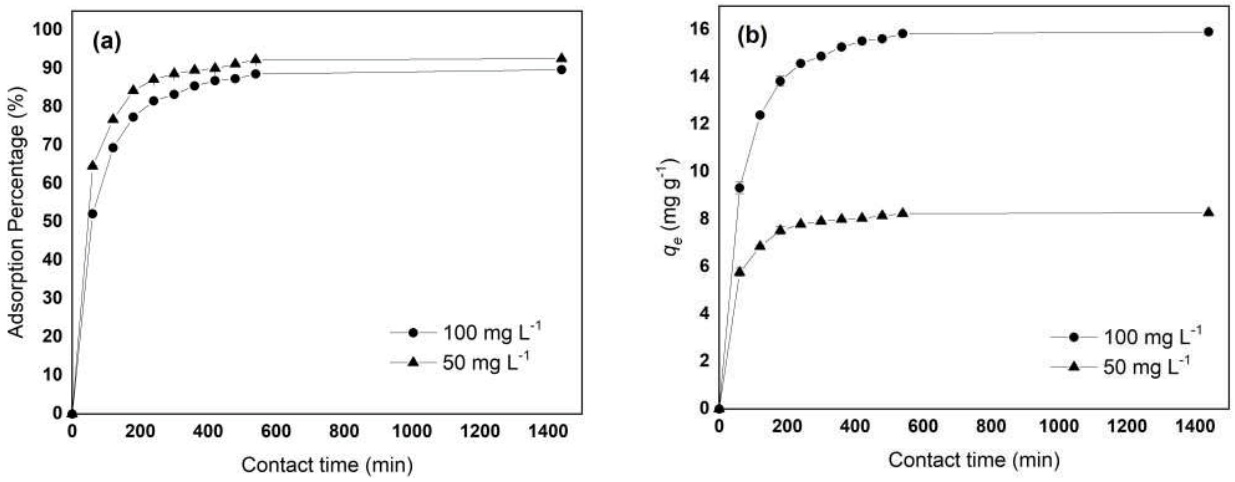

Fig. 5. Kinetics of rhodamine B adsorption on eucalyptus sawdust. (a) Adsorption percentage and (b) adsorption capacity.

Adsorption capacity is related to the final concentration of dye in the liquid phase (Fig. 7a). By plotting experimental data onto a graph, we obtained a concave curve. According to the classification of McCabe et al. [32], this shape indicates that adsorption is highly favorable: large quantities of adsorbate can be adsorbed by low concentrations of adsorbent. In this case, the mass of dye retained per unit of ES is high for low equilibrium concentrations of the dye in liquid phase. In line with the classification of Giles et al. [33], there was high affinity between absorbate and adsorbent, indicating the occurrence of chemisorption and exchange or sharing of electrons between RhB and ES surface.

For a better understanding of the RhB adsorption process, we fitted Langmuir and Freundlich isotherm models

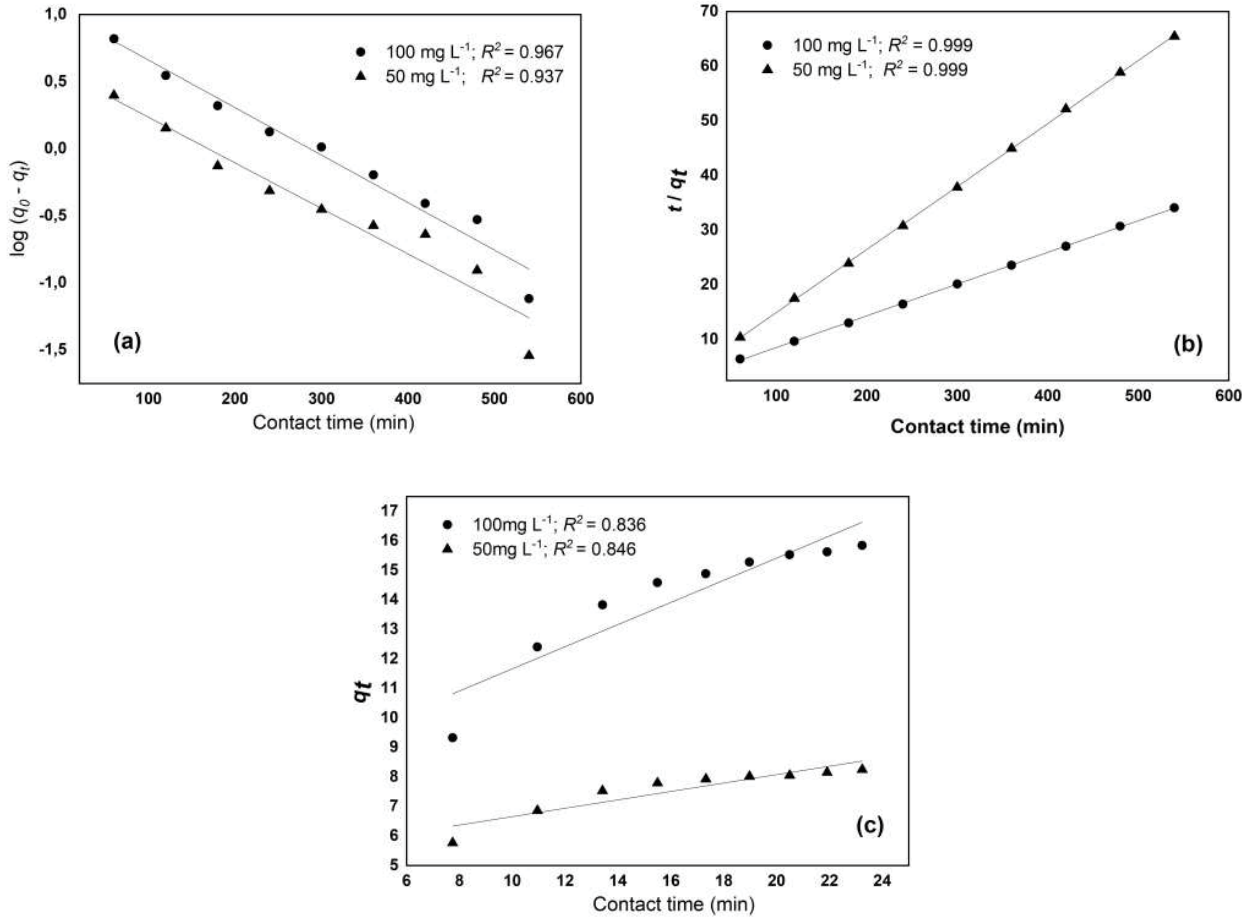

Fig. 6. Experimental data of rhodamine B adsorption fitted by (a) pseudo-first order, (b) pseudo-second-order, and (c) intraparticle diffusion kinetic models.

Table 6
Kinetic parameters of rhodamine B adsorption on eucalyptus sawdust

Kinectic model	C_0 (mg L^{-1})	$q_{e,calc}$ (mg g^{-1})	k	R^2
Pseudo-first-order	100	10.34	0.0081 min^{-1}	0.9672
	50	3.75	0.0078 min^{-1}	0.9369
Pseudo-second-order	100	17.24	0.0012 g mg^{-1} min^{-1}	0.9998
	50	8.67	0.0039 g mg^{-1} min^{-1}	0.9999
Intraparticle diffusion	100	–	0.3750 mg g^{-1} $min^{-0.5}$	0.8566
	50	–	0.1422 mg g^{-1} $min^{-0.5}$	0.8458

to experimental data (Fig. 7), allowing estimation of adsorption parameters and correlation coefficients (Table 7). Langmuir isotherm model showed the best fit to the data (R^2 = 0.9947). The Langmuir constant was 5.4379 L mg^{-1} and the maximum adsorption capacity 29.94 mg g^{-1}.

3.5. Thermodynamic parameters

A thermodynamic study was performed at three different temperatures. First, adsorption equilibrium constants (Table 8) were determined by plotting ($C_0 - C_e$) vs. C_e. Linear regression afforded the linear van't Hoff equation, which was used to determine ΔG°_{ads}, ΔS°_{ads}, and ΔH°_{ads} (Table 9). The adopted gas constant (R) was 8.3145 kJ mol^{-1} K^{-1}.

Gibbs energy variation values revealed that RhB adsorption on ES is spontaneous and favorable ($\Delta G^\circ_{ads} < 0$). It was also possible to verify that, by increasing the temperature, reaction spontaneity also increases. This is indicated by the increase in Gibbs energy negativity. Enthalpy variation showed that the process is endothermic ($\Delta H^\circ_{ads} > 0$), which is in agreement with the values of Gibbs energy, given that an increase in temperature favors adsorption.

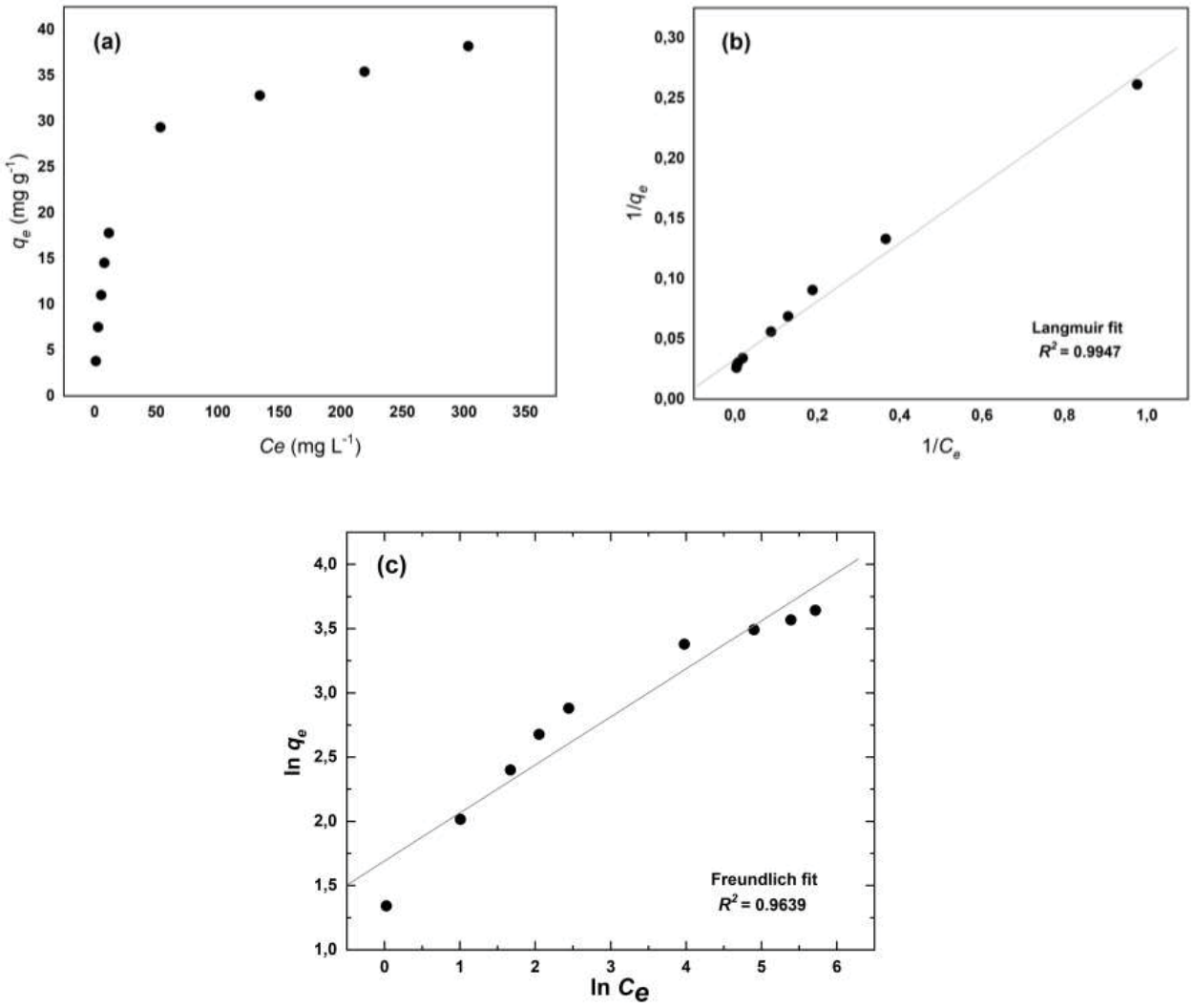

Fig. 7. (a) Adsorption isotherm and experimental data fitted by the (b) Langmuir and (c) Freundlich models.

Table 7
Langmuir and Freundlich parameters for rhodamine B adsorption on eucalyptus sawdust

Model	Parameter
Langmuir	q_{max} = 29.94 mg g^{-1}
	K_L = 0.1386 L mg^{-1}
	R_L = 0.014–0.268
	R^2 = 0.9947
Freundlich	K_F = 5.4379
	n = 2.68
	R^2 = 0.9639

Physisorption is indicated by enthalpy values of 2.09 to 20.9 kJ mol^{-1}, whereas chemisorption is indicated by values of 20.9 to 418.4 kJ mol^{-1}. Therefore, according to the final enthalpy value obtained in this study (ΔH°_{ads} = 38.31 kJ mol^{-1}), RhB adsorption on ES is a chemical process.

Table 8
Adsorption equilibrium constants at the three studied temperatures

Temperature	K_{ads}
30°C (303 K)	1.249
40°C (313 K)	2.145
50°C (323 K)	3.139

The positive entropy variation suggests that the solid–liquid interface disorder increases with structural changes in adsorbate and adsorbent. A positive variation of entropy in an adsorption reaction with negative Gibbs energy variation indicates that the adsorbate has high affinity for the adsorbent.

Previous research has carried out kinetic, isotherm, and thermodynamic studies of RhB adsorption on different biosorbents. Da Rosa et al. [15] used the green microalga

Table 9
Thermodynamic parameters for rhodamine B adsorption on eucalyptus sawdust

	Parameter			
Temperature	ΔG°_{ads} (kJ mol^{-1})	ΔH°_{ads} (kJ mol^{-1})	ΔS°_{ads} (J mol^{-1})	R^2
30°C (303 K)	−609.83			
40°C (313 K)	−1,894.34	38.31	128.45	0.9950
50°C (323 K)	−3,178.86			

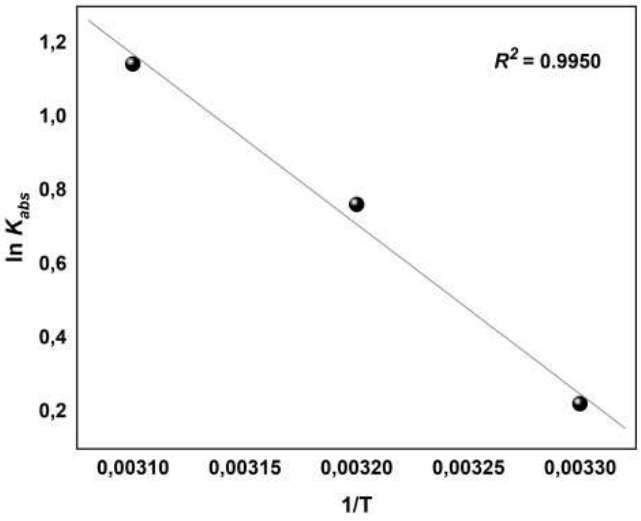

Fig. 8. Van't Hoff's plot for rhodamine B adsorption on eucalyptus sawdust.

Chlorella pyrenoidosa to remove RhB dye from stone dyeing wastewater. The maximum biosorption capacities at 25°C, 35°C, and 45°C were 63.14, 53.46, and 54.20 mg g^{-1}, respectively, and the Sips isotherm model had the best fit to experimental data. The authors showed that an increase in temperature had a negative effect on biosorption capacity. Khamparia et al. [18] investigated the RhB adsorption potential of a natural adsorbent, *Xanthium strumarium* seed hull. The Freundlich isotherm model showed a good fit to experimental data, indicating multilayer adsorption. The kinetic model that best described the process was the pseudo-second-order model. Thermodynamic studies suggested that adsorption, characterized as physisorption, was favored at high temperatures. At the optimum pH, 75% of RhB was removed using only 0.05 g of adsorbent per 25 mL of solution; that is, the maximum biosorption capacity was 2 mg g^{-1}. Saigl and Ahmed [34] used pomegranate peel powder for RhB adsorption. The maximum biosorption capacity was 7.37 mg g^{-1}. Adsorption kinetics were explained by a pseudo-second-order model, and equilibrium data were well described by the Langmuir equation. Thermodynamic parameters confirmed the endothermic behavior of RhB adsorption on pomegranate peel powder. In this study, ES presented a maximum adsorption capacity of 29.94 mg g^{-1}, which corresponds to a capacity greater than *Xanthium strumarium* [18] and pomegranate peel [34].

It is worth mentioning that, in the vast majority of studies, adsorption is spontaneous and favorable. The pseudo-second-order model best describes the adsorptive process of RhB. The model considers that adsorption rate depends on the amount of solute adsorbed on the adsorbent surface and the amount adsorbed at equilibrium. Regarding adsorption isotherms, there appears to be no pattern of models; the most adequate model depends on the biosorbent used. This fact can be explained by differences in surface characteristics (morphology and functional groups) of biosorbents, resulting in different adsorption mechanisms. In the case of ES, the Langmuir adsorption isotherm best explained the reaction. The model describes adsorption on homogeneous sites of an adsorbent in monolayers, which means that the surface contains a fixed number of adsorption sites. We believe this mechanism prevailed because ES has a low surface area, impairing multilayer biosorption.

4. Conclusions

ES exhibited a good capacity to decolorize RhB in aqueous solutions. The effects of biomass particle size, biomass dosage, and solution pH were evaluated. Experimental results and statistical analysis showed that only biomass dosage significantly influenced the adsorption process. The Langmuir isotherm model provided the best fit to data. The adsorption reaction followed second-order kinetics, and diffusion was the rate-determining step. Thermodynamic studies suggested that the reaction should be carried out at high temperatures, as it is an endothermic process. A dye removal percentage of 92.6% was achieved using 1.05 g of ES per 50 mL of RhB. The findings were validated by statistical analysis, resulting in an accurate conclusion about the mechanism of RhB adsorption, thereby confirming the capacity of ES to remove RhB from aqueous solution.

References

[1] S. Singh, N. Parveen, H. Gupta, Adsorptive decontamination of rhodamine-B from water using banana peel powder: a biosorbent, Environ. Technol. Innovation, 12 (2018) 189–195.
[2] B. Kraeutler, A.J. Bard, Heterogeneous photocatalytic decomposition of saturated carboxylic-acids on TiO_2 powder: decarboxylative route to alkanes, J. Am. Chem. Soc., 100 (1978) 5985–5982.
[3] P. Wang, M. Du, H. Zhu, S. Bao, T. Yang, M. Zou, Structure regulation of silica nanotubes and their adsorption behaviors for heavy metal ions: pH effect, kinetics, isotherms and mechanism, J. Hazard. Mater., 286 (2015) 533–544.
[4] T. Kudo, Y. Nakamura, A. Ruike, Development of rectangular column structured titanium oxide photocatalysts anchored on

silica sheets by a wet process, Res. Chem. Intermed., 29 (2003) 631–639.
[5] D. Bahnemann, Photocatalytic water treatment: solar energy applications, Sol. Energy, 77 (2004) 445–459.
[6] O. Carp, C.L. Huisman, A. Reller, Photoinduced reactivity of titanium dioxide, Prog. Solid State Chem., 32 (2004) 33–177.
[7] H. Xu, Y. Zhang, Q. Jiang, N. Reddy, Y. Yang, Biodegradable hollow zein nanoparticles for removal of reactive dyes from wastewater, J. Environ. Manage., 125 (2013) 33–40.
[8] P.A. Carneiro, M.E. Osugi, J.J. Sene, M.A. Anderson, M.V.B. Zanoni, Evaluation of color removal and degradation of a reactive textile azo dye on nanoporous TiO_2 thin-film electrodes, Electrochim. Acta, 49 (2004) 3807–3820.
[9] V.K. Gupta, I. Ali, T.A. Saleh, A. Nayak, S. Agarwal, Chemical treatment technologies for waste-water recycling - an overview, RSC Adv., 16 (2012) 6380–6388.
[10] G. Crini, Non-conventional low-cost adsorbents for dye removal: a review, Bioresour. Technol., 97 (2006) 1061–1085.
[11] M. Tuzen, A. Sari, T.A. Saleh, Response surface optimization, kinetic and thermodynamic studies for effective removal of rhodamine B by magnetic AC/CeO_2 nanocomposite, J. Environ. Manage., 206 (2018) 170–177.
[12] H.A. Kiwaan, T.M. Atwee, E.A. Azab, A.A. El-Bindary, Photocatalytic degradation of organic dyes in the presence of nanostructured titanium dioxide, J. Mol. Struct., 1200 (2020) 1–11.
[13] A.A. Abdulrazak, S. Rohani, Sodium dodecyl sulfate-modified Fe_2O_3/molecular sieves for removal of rhodamine B dyes, Adv. Mater. Sci. Eng., 2018 (2018) 1–10.
[14] M.P. Koniarz, J. Goscianska, R. Pietrzak, Removal of rhodamine B from water by modified carbon xerogels. Colloids Surf., A, 543 (2018) 109–117.
[15] A.L.D. Da Rosa, E. Carissimi, G.L. Dotto, H. Sander, L.A. Feris, Biosorption of rhodamine B dye from dyeing stones effluents using the green microalgae *Chlorella pyrenoidosa*, J. Cleaner Prod., 198 (2018) 1302–1310.
[16] H. Li, N. Li, J. Jiang, D. Chen, Q. Xu, H. Li, J. Lu, Molecularly imprinted magnetic microparticles for the simultaneous detection and extraction of rhodamine B, Sens. Actuators, B, 246 (2017) 286–292.
[17] H. Zeng, M. Gao, T. Shen, F. Ding, Modification of silica nanosheets by Gemini surfactants with different spacers and its superb adsorption for rhodamine B, Colloids Surf., A, 555 (2018) 746–753.
[18] S. Khamparia, D.K. Jaspal, *Xanthium strumarium* L. seed hull as a zero cost alternative for rhodamine B dye removal, J. Environ. Manage., 197 (2017) 498–506.
[19] W.S.W. Nagah, M.A.K.M. Hanafiah, Biosorption of copper ions from dilute aqueous solutions on base treated rubber (*Hevea brasiliensis*) leaves powder: kinetics, isotherm, and biosorption mechanisms, J. Environ. Sci., 20 (2008) 1168–1176.
[20] T.C. Sarker, S.M.G.G. Azam, A.M. Am El-Gawad, S.A. Gaglione, G. Bonanomi, Sugarcane bagasse: a potential low-cost biosorbent for the removal of hazardous materials, Clean Technol. Environ. Policy, 19 (2017) 2343–2362.
[21] A. Stavrinou, C.A. Aggelopoulos, C.D. Tsakiroglou, Exploring the adsorption mechanisms of cationic and anionic dyes onto agricultural waste peels of banana, cucumber and potato: adsorption kinetics and equilibrium isotherms as a tool, J. Environ. Chem. Eng., 6 (2018) 6958–6970.
[22] Y. Dai, Q. Sun, W. Wang, L. Lu, M. Liu, J. Li, Y. Zhang, Utilizations of agricultural waste as adsorbent for the removal of contaminants: a review, Chemosphere, 211 (2018) 235–253.
[23] S.N. Jain, P.R. Gogate, Efficient removal of Acid Green 25 dye from wastewater using activated *Prunus dulcis* as biosorbent: batch and column studies, J. Environ. Manage., 210 (2018) 226–238.
[24] S.N. Jain, P.R. Gogate, Acid Blue 113 removal from aqueous solution using novel biosorbent based on NaOH treated and surfactant modified fallen leaves of *Prunus dulcis*, J. Environ. Chem. Eng., 5 (2017) 3384–3394.
[25] S.N. Jain, P.R. Gogate, Adsorptive removal of azo dye in a continuous column operation using biosorbent based on NaOH and surfactant activation of *Prunus dulcis* leaves, Desal. Water Treat., 141 (2019) 331–341.
[26] V.S. Tran, H.H. Ngo, W. Guo, J. Zhang, S. Liang, C. Ton-That, X. Zhang, Typical low-cost biosorbents for adsorptive removal of specific organic pollutants from water, Bioresour. Technol., 182 (2015) 353–363.
[27] A.P.S. Morais, C.A. Sansígolo, M.O. Neto, Effects of autohydrolysis of *Eucalyptus urograndis* and *Eucalyptus grandis* on influence of chemical components and crystallinity index, Bioresour. Technol., 214 (2016) 623–628.
[28] J. Zheng, Y. Tashiro, Q. Wang, K. Sakai, K. Sonomoto, Feasibility of acetone–butanol–ethanol fermentation from eucalyptus hydrolysate without nutrients supplementation, Appl. Energy, 140 (2015) 113–119.
[29] L.N. dos Santos, H.C. Fernandes, R.M.F. Silva, M.L. da Silva, A.P. de Souza, Evaluation of costs of harvester in cut and processing of eucalyptus wood, Revista Árvore, 41 (2017) 1–9.
[30] A. Revil, P.A. Pezard, P.W.J. Glover, Streaming potential in porous media 1. Theory of the zeta potential, J. Geophys. Res.: Solid Earth, 104 (2019) 20021–20031.
[31] F.H.M. Souza, V.F.C. Leme, G.O.B. Costa, K.C. Castro, T.R. Giraldi, G.S.S. Andrade, Biosorption of rhodamine B using a low-cost biosorbent prepared from inactivated *Aspergillus oryzae* cells: kinetic, equilibrium and thermodynamic studies, Water Air Soil Pollut., 231 (2020) 1–13.
[32] W.L. Mccabe, J.C. Smith, P. Harriot, Units Operations of Chemical Engineering, 5th ed., McGraw Hill, New York, 1993.
[33] C.H. Giles, T.H. Macewan, S.N. Nakhwa, D. Smith, Studies in adsorption – Part XI: a system of classification of solution adsorption isotherms, and its use in diagnosis of adsorption mechanisms and in measurement of specific surface areas of solids, J. Chem. Soc. (London), 846 (1960) 3973–3993.
[34] Z.M. Saigl, A.M. Ahmed, Separation of rhodamine B dye from aqueous media using natural pomegranate peels, Indones. J. Chem., 21 (2021) 212–224.